Use of Satellite and In Situ Reflectance Data for Lake Water Color Characterization in the Everest Himalayan Region

Authors: Matta, Erica, Giardino, Claudia, Boggero, Angela, and Bresciani, Mariano

Use of Satellite and In Situ Reflectance Data for Lake Water Color Characterization in the Everest Himalayan Region

Erica Matta[1], Claudia Giardino[1]*, Angela Boggero[2], and Mariano Bresciani[1]

* Corresponding author: giardino.c@irea.cnr.it

[1] *Optical Remote Sensing Group, National Research Council-Institute for Electromagnetic Sensing of the Environment CNR-IREA, Via Bassini 15, 20133 Milano, Italy*
[2] *National Research Council-Institute of Ecosystem Study CNR-ISE, Largo Tonolli 50, 28922 Verbania Pallanza, Italy*

This study applied remote sensing techniques to the study of water color in Himalayan glacial lakes as a proxy of suspended solid load. In situ measurements gathered in 5 lakes in October 2014 during satellite data acquisition enabled the characterization of water reflectance and clarity and supported image processing. Field data analysis led to a distinction between 3 water colors and a consequent lake water color classification on a regional scale from Landsat-8 data previously corrected for atmospheric and adjacency effects. Several morphometric parameters (lake size and shape, distance between lake and glacier) were also computed for the lakes thus classified. The results showed spatial and temporal variations in lake water color, suggestive of relationships between glacier shrinkage and the presence of brighter and more turbid water. A finer-scale analysis of the spatial variability of water reflectance on Chola Lake (based on GeoEye-1 data captured on 18 October 2014) showed the contribution of water component absorption from the inflow. Overall, the findings support further research to monitor Himalayan lakes using both Landsat-8 and Sentinel-2 (with its improved resolutions).

Keywords: *Hyperspectral water reflectance; lake color; lake size and shape, high spatial resolution; Landsat; Secchi disk; glacial lakes; glacial lake outburst flood (GLOF); Nepal.*

Peer-reviewed: *July 2016*   ***Accepted:*** *October 2016*

Introduction

Climate change is known to affect glacier mass balances and lead to a net loss of ice, due mainly to higher temperatures and declining precipitation (Salerno et al 2008; Wu et al 2012; Thakuri et al 2014). The rising melting rates induced by climate change can have various effects, including an increase in the number and size of glacial lakes (Thompson et al 2012) and the creation of potentially dangerous lakes with a risk of outburst floods (Bolch et al 2008). Meltwater from glaciers is the main factor determining lake volume in the region, but it also carries glacial sediment into the lakes, increasing their turbidity (eg Irwin 1974; Robinson and Matthaei 2007). Glacial meltwater can alter chemical processes in glacial lakes, for instance increasing water conductivity and ionic concentrations (Thies et al 2007; Lami et al 2010). Sediment-rich water becomes less transparent, inhibiting primary production and making it hard for higher organisms in the food web to survive in the lake (Koenings et al 1990). All these changes have been underway in mountainous regions where there are glaciers, and it is important to monitor the close interactions between glaciers and glacial lakes.

For glacial lakes in remote and relatively inaccessible areas, it is impractical to characterize these interactions by means of conventional fieldwork. Remote sensing has become a powerful and convenient option for ongoing synoptic measurements and their retrospective analysis. Satellite data have been widely used to study lakes at high altitudes, in particular in the Himalayas. Recent examples of the use of satellite data on the Himalayan region can be found in Raj and Kumar (2016), who describe the evolution of glacial lakes in the Uttarakhand Himalaya; Raj et al (2013), who produced an inventory of the glacial lakes in the Sikkim Himalaya; Giardino et al (2010), who mapped the suspended particulate matter in lakes in the Mount Everest region; Quincey et al (2007), who identified glacial lake hazards in the Himalayas; and Kargel et al (2005), who found a supraglacial lake on Rongbuk Glacier.

In the present study, satellite data were used to examine the optical characteristics of Himalayan lakes in terms of their radiometric properties, such as reflectance or water color, identifiable by remote sensing. The size of the particles in suspension in the lake and their numerical

density change, depending on the influx of water from the glacier; this affects light interaction and lake color. Higher turbidity levels make these lakes look gray, whereas lakes with a lower input of particles in suspension from the glacier appear dark blue (Kargel et al 2005). Lakes with large amounts of suspended sediment generally have a higher visible reflectance than clear waters (Bukata et al 1995). Once satellite data have been corrected for atmospheric effects, changes in water reflectance signals from visible to near-infrared wavelengths depend on differences in the water components in the upper layer of the water body. These variations can be retrieved by applying specific algorithms (eg Odermatt et al 2010; Gholizadeh et al 2016) built on empirical or semiempirical methods that use reflectance at appropriate wavebands as correlates, or by means of such semianalytical and quasi-analytical approaches as spectral inversion, which relies on matching spectral data with bio-optical forward models. Whatever the approach, the calibration and validation of such models take advantage of the availability of site-specific data gathered in the field. For instance, in situ radiometric data have been used to tune suitable regional algorithms for measuring water quality parameters (eg Hommersom et al 2011) and to assess the performance of atmospheric correction methods adopted to obtain water reflectance data from satellite images (eg Brando et al 2016).

The aim of the present work was to characterize the water reflectance in the visible near-infrared (VIS-NIR) region of glacial lakes in the Mount Everest region (Nepal) as a proxy of their color, using in situ radiometric data and satellite acquisitions. During fieldwork in October 2014, the water reflectance of 5 Himalayan lakes was measured at the same time as data were acquired by 2 satellites, GeoEye-1 and Landsat-8. The data from GeoEye-1, with its higher spatial resolution (2 m), enabled water color variability to be assessed within a single lake, whereas the Landsat-8 image at 30 m resolution documented the color variability between different lakes in the region. The classification of the lakes based on the Landsat-8 data is analyzed here in relation to their morphometric parameters (lake size and shape, distance of lake from glacier), and considering the lake color classification proposed by Giardino et al (2010), in an effort to explain recent lake color variations in the region.

Study area

The study area is between 27.6–28.3°N and 86.3–87.1°E, and includes both Nepali and Chinese territory (Figure 1). In the center of this area is the Sagarmatha National Park (SNP), the highest protected area in the world, a UNESCO World Heritage Site since 1979. The SNP is situated in the Solu-Khumbu district and covers 1141 km^2 in northeastern Nepal. The area is dominated by Mount Everest and 7 other peaks over 7000 m high, and it is the main source of freshwater for the Nepali people downstream.

The glaciers are largely covered in debris, and this alters the energy exchanges between ice and atmosphere (Mattson et al 1993). The area's glacial lakes have different origins and are differently connected with the glaciers: some just formed as melting ponds above the glacier's tongue (supraglacial); some are moraine dammed and emerge directly from the glacier's front (proglacial); and some are not connected directly to a glacier but share the same basin (cirque). Proglacial lakes are considered the most dangerous in the event of major melting of the glaciers behind them because of the risk of outburst floods—as already seen in some lakes in the SNP, such as Nare Drangka in 1977 (Buchroithner et al 1982) and Dig Tsho in 1985 (Vuichard and Zimmermann 1987). The lakes in the study area lie between approximately 4000 and 5700 m above sea level, well above the tree limit, and they are fed mainly by perennial snow and ice.

The climate in the SNP is driven by the Indian monsoon, with successions of dry and wet seasons. Most of the annual precipitation (80%) falls between June and September. The winter is normally dry, though occasional cyclones can cause heavy snowfall (Ueno et al 2001). One such exceptional event occurred during fieldwork in October 2014, when Cyclone Hudhud, originating in the Andaman Sea (Bay of Bengal), intensified on its way toward India, developing into a severe storm and causing several deaths in India (Andhra Pradesh) and Nepal (Annapurna region).

Five lakes in the Khumbu and Imja valleys with different basin morphologies were selected for fieldwork (Table 1 and Figure 1). These lakes are here identified by a univocal sequential code, which is the lake cadastral number (LCN), as assigned by Tartari et al (1997, 2008) in their inventory and surface change detection studies. Lakes LCN9 and LCN10 are located above the CNR-EvK2 Pyramid observatory and constitute a cascade system, with the upper lake feeding the lower one. Lake LCN24 (Chola) is dammed by a lateral moraine separate from the lake basin that conceals the outlet, so the water emerges some meters below the lake. Lake LCN31 is a semicircular lake formed at the end of the Duwo glacier moraine. Lake LCN161 (Imja) began as a small meltwater pond in the 1960s, but has developed into a proglacial lake, raising concern about its stability and the risk of outburst flooding (Bolch et al 2008; Byers et al 2013). The Imja Glacier's ice tongue protrudes into the water, directly feeding the lake. It is a typical proglacial lake, gradually expanding over the years as the glacier melts and retreats. It now poses a threat to the local population (Bajracharya et al 2007) because its basin consists of low sloping glacier surfaces and it collects the meltwater from 3 surrounding glacier tongues, so a moraine break or snow/ice avalanches could have catastrophic consequences. For the other lakes within the study area (see Figure 1), most of those within

FIGURE 1 Map of the study site. Lakes inside SNP are coded with cadastral numbers (1–200) based on Tartari et al (1997, 2008), and other lakes are coded with randomly assigned numbers (beginning at 1001). (Map by the authors)
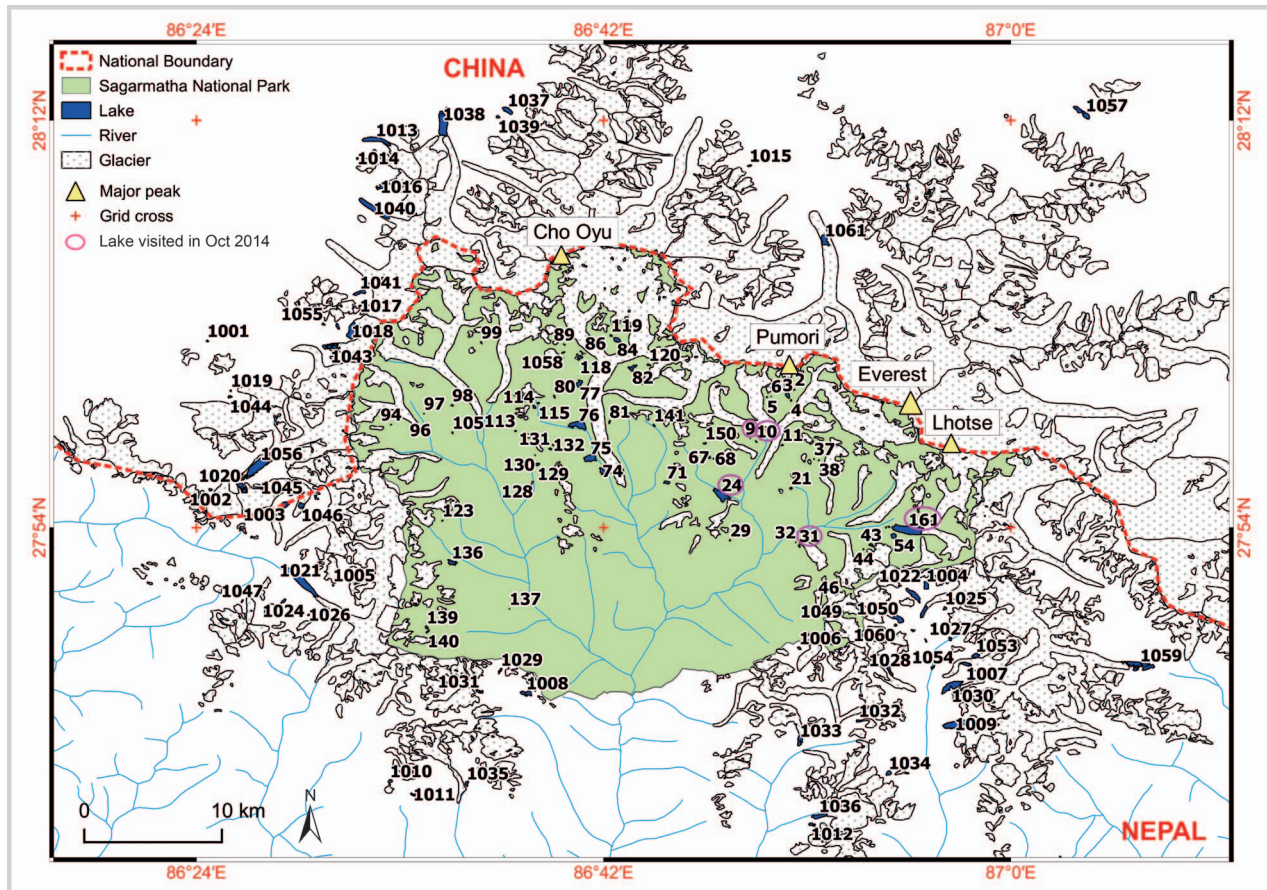
the SNP and characterized by previously described basin morphologies, the overall assessment concerning their risk of outburst is then conducted by using satellite observations.

Material and methods

Field data

Fieldwork was conducted from 14 to 20 October 2014 to collect radiometric and transparency data on 5 lakes between 4532 and 5067 m above sea level (Table 1). Radiometric measurements were taken with a field spectroradiometer (WISP-3, WaterInsight), and water transparency was measured using a Secchi disk (SD) to determine the depth to which visibility remained clear. WISP-3 simultaneously records radiance (40° sky and 40° water) and irradiance spectra in the 400–800 nm range (Hommersom et al 2012). To avoid any influence of the lake bottom on the radiometric measurements, sampling stations were located in areas of deep open water reached

TABLE 1 Morphological characteristics of sampled lakes. Morphology is based on Tartari et al (2008).

Lake cadastral number	Elevation (m)	Area (km^2)	Perimeter (m)	Valley	Feeding glacier/river	Morphology
LCN9	5213	0.008	146	Khumbu	No name	Cirque
LCN10	5067	0.017	207	Khumbu	No name	Cirque
LCN24	4532	0.509	1556	Khumbu	Cholo Khola river	Moraine dammed
LCN31	4688	0.037	373	Imja	Duwo glacier	Cirque
LCN161	5022	1.05	2402	Imja	Ambulapcha, Imja, and Lhotse Shar glaciers	Proglacial

with an inflatable boat. For each station, a water sample was collected and analyzed with an iQwtr instrument (Ghezehegn et al 2014), which uses an innovative, low-cost, user-friendly field application to estimate surface water turbidity from photos taken with smartphones (BlueLeg Monitor and WaterInsight).

Satellite images

Two images were acquired by the GeoEye-1 and Landsat-8 Operation Land Imager (OLI) satellite sensors on 18 and 29 October 2014, respectively. The GeoEye-1 acquisition was concurrent with in situ measurements obtained on Lake LCN24. Both sensors are multispectral, with typical blue, green, red, and infrared channels.

For both images, radiometric calibration and correction for atmospheric effects were performed to obtain surface reflectance data. In particular, radiometric correction of the OLI image was based on the specific coefficients suggested by Pahlevan et al (2014) for water applications. The vector version of the 6S code (Second Simulation of a Satellite Signal in the Solar Spectrum) (Vermote et al 1997) was applied to the satellite images to correct for atmospheric effects and measure water reflectance. The atmospheric profile was established from user-defined ozone and water vapor values (Ozone Over Your House, NASA and AERONET station EVK2__CNR), and the continental aerosol model was adopted as the most representative of the study site. The aerosol optical depth was derived from AERONET data (EVK2__CNR station) and set to 0.05. The 6S-derived reflectance values were further corrected for adjacency effects based on the residual between the 6S-derived reflectance from the GeoEye-1 image and the synchronous WISP-3 in situ data obtained for Lake Chola (LCN24).

Three thresholds were chosen to classify the lakes by water color on the corrected Landsat-8 data, based on intensity of water reflectance (r_w) and on the observed desaturation of lake colors from dark blue to turquoise to gray (according to Giardino et al 2010): $r_{wVIS\_NIR} < 10\%$ for clear blue waters (as in lakes LCN10 and LCN31), $10\% < r_{wVIS\_NIR} < 20\%$ for turquoise lakes (like LCN24); and $r_{wVIS\_NIR} > 20\%$ for gray, sediment-rich waters (as in LCN161). The value of r_{wVIS_NIR} was calculated from the sum of the r_w values (Bukata et al 1995) in the typical VIS-NIR band settings of multispectral sensors like the GeoEye-1 and OLI. For the classified lakes, the shape index proposed by Frohn (2006)—which has been judged to perform well for raster-derived data (Bogaert et al 2000)—was used to test the relationship between a lake's water color and its shape. The shape index defined by Frohn ranges between 0 (for a square lake) and 1 (for a lake more complex in shape). The distances between lake and glacier were also computed on the basis of the Randolph glacier inventory (Arendt et al 2014) using

FIGURE 2 Reflectance (r_w) spectra measured with the WISP-3 field spectroradiometer during fieldwork. Note that LCN9 and LCN10 are spectrally identical. Measured SD depths are indicated close to each spectrum. (-) means dimensionless.
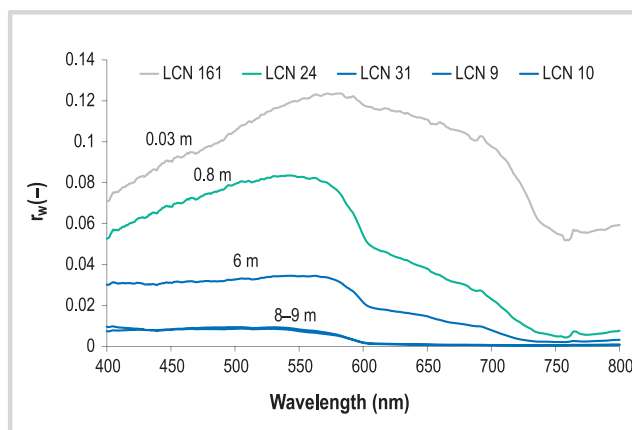
instruments commonly available in geographic information systems.

On a finer scale, the r_w values measured in the 545 nm GeoEye-1 band were used to analyze spatial variations in the LCN24 lake, because this spectral band is known to be affected by organic and inorganic sediment in suspension (Kirk 2011).

Results

The WISP-3 r_w spectra and SD measurements for the 5 surveyed lakes are shown in Figure 2. Overall, 3 groups of spectra with increasing degrees of brightness were clearly distinguishable by water color. LCN9 and LCN10 are spectrally identical highly transparent lakes with dark blue waters and similar SD depths (about 8–9 m). LCN31 is also a clear lake with a bluish color and reflectance values decreasing from blue toward longer wavelengths because of water absorption. LCN24 and LCN161 have r_w spectra typical of higher turbidity levels, as confirmed by the SD depths lower than 1 m. The highest reflectance was measured in LCN161, which looked gray during fieldwork observations, with clearly visible patterns of suspended sediment. Field measurements of total suspended matter concentrations obtained in October 2008 (Giardino et al 2010) support the observed radiometric differences: the total suspended-matter values ranged from 0.63 g m^{-3} for lake LCN10 to 102 g m^{-3} for lake LCN161, with intermediate values of 1.7 g m^{-3} and 6.69 g m^{-3} for lakes LCN31 and LCN24, respectively. The WISP-3 r_w spectra for 4 lakes (all except LCN9) were comparable with the ALOS-derived reflectance of Figure 2 in Giardino et al (2010). The average r_w in situ data in the VIS-NIR were then compared with the SD values, and a correlation was identified ($r^2 = 0.85$). The transparency values obtained with the SD (cf. Figure 2) and the iQwtr also revealed a good correlation ($r^2 = 0.94$).

When compared with in situ radiometric measurements, the 6S-derived reflectance showed the

FIGURE 3 Water color classification of the 119 investigated lakes. Each bar shows the percentage of pixels classified as blue, turquoise, or gray water for 1 lake. Lake codes are on the left and right; asterisks indicate lakes located in China.
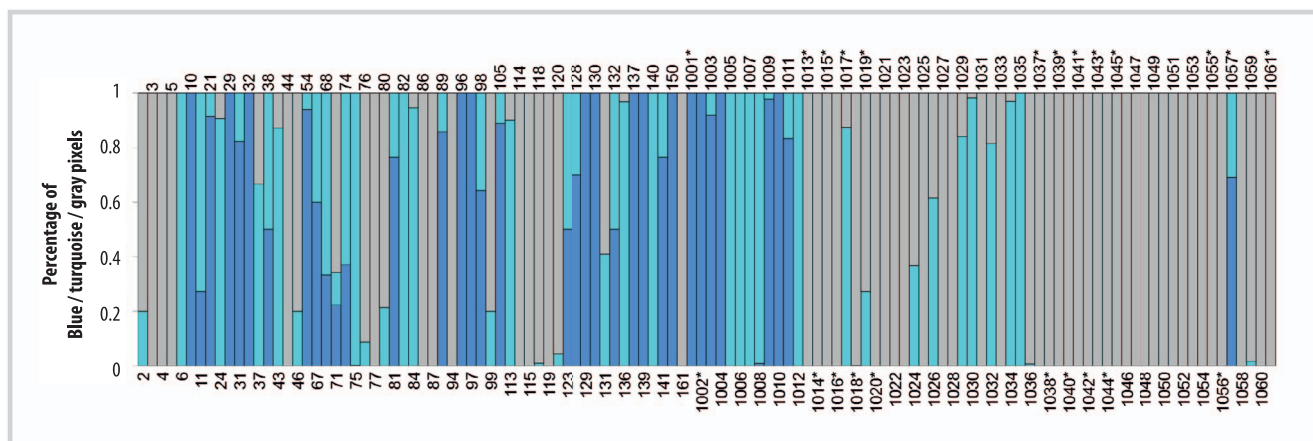
same trend, but with a higher magnitude. This difference in spectral magnitude was attributed to adjacency effects due to fresh snow falling on 14 October 2014, a few days before the Landsat-8 and GeoEye-1 data were acquired. This effect increased the signal by 39% (more in the blue band, and less toward the NIR), a finding generally consistent with the report from Bélanger et al (2007) of an adjacency effect due to sea ice resulting in a similar overestimation of the water-leaving reflectance. To correct for adjacency effects, the 6S-derived reflectance obtained with the Landsat-8 and GeoEye-1 data was adjusted to the WISP-3 in situ data for Lake Chola (LCN24), taken for reference because the field and satellite data collection coincided.

The 3 r_{wVIS_NIR} thresholds defined in the previous section were applied to OLI data and corrected for atmospheric and adjacency effects to classify the lakes. Figure 3 shows the outcome of the classification procedure for 119 lakes. Of the lakes, 52% have mainly (>50% of pixels) gray waters, 24% have mainly blue waters, and 21% have mainly turquoise waters; 3% have mixed colors (half blue and half turquoise). The lakes in

Nepal (96 of 119) have a greater diversity of water colors, largely gray (45%) with fewer blue (27%) and turquoise (25%) (the remaining 3% were classified with mixed colors), whereas the Chinese lakes (23 of 119) have a preponderance of gray waters (83%) and even fewer blue (13%) or turquoise (4%). When the classification obtained on the OLI image was compared with one previously obtained on an ALOS image (Giardino et al 2010) for 116 lakes in the area (which is the maximum number of lakes commonly detectable—i.e. included in both scene swaths—and free from cloud cover in both images), 71% of the lakes revealed differences in the percentage composition of their water color over time, the waters tending to become clearer in 38% of the lakes and more turbid in 62%.

Figure 4 compares water color and lake size and shape. Lakes with turquoise and gray water were generally larger than the blue lakes. The lakes with gray water could have a surface area in excess of 1 km^2, indicating relatively large water volumes capable of causing damage in the event of an outburst flood. The shift from blue to gray water coincided with a declining likelihood of a lake being

FIGURE 4 Distribution of water color by lake size and shape index (Frohn 2006). The shape index ranges between 0 (circular shape) and 1 (irregular shape). Box plots show 25th and 75th percentiles; error bars show 10th and 90th percentiles; diamonds show outlier values.
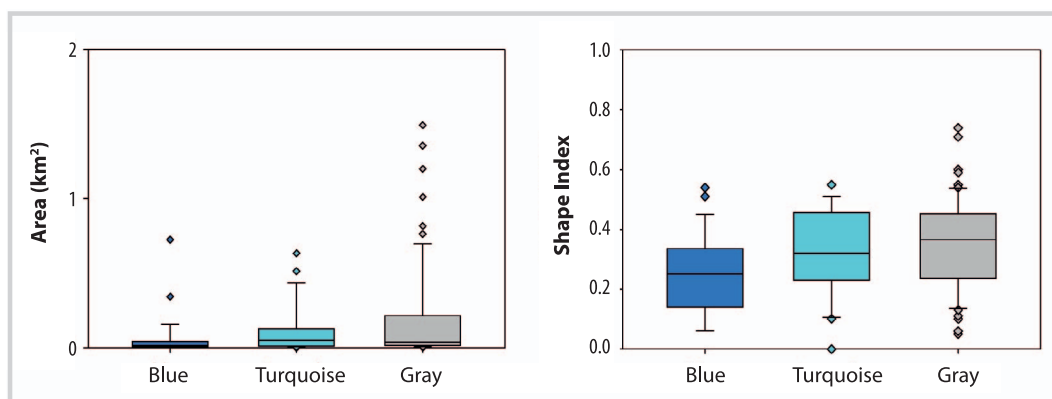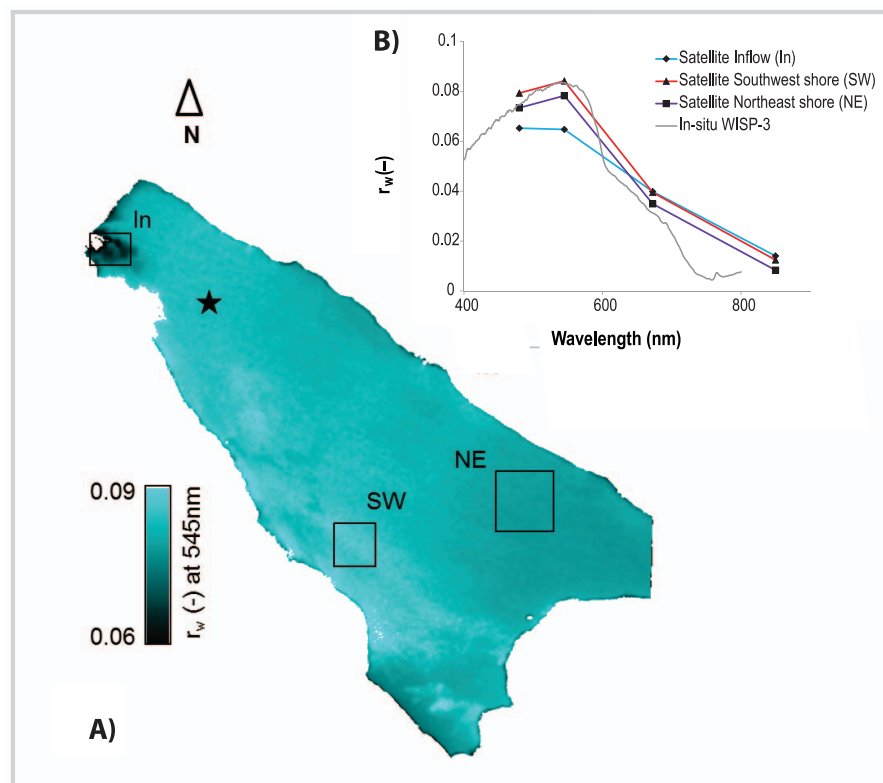
FIGURE 5 Lake Chola (LCN24): (A) map showing r_w values in the 545-nm band, captured by GeoEye-1; (B) r_w values in the 400–800-nm range of 3 lake zones, with different reflectance characteristics, captured by GeoEye-1, and r_w values in the 400–800-nm range measured with WISP-3 in the location marked with a star. (-) means dimensionless.

square (ie shape index values approaching 1). Lakes with gray and turquoise water were closer to their glaciers than those with blue water (median <0.25 km for gray-water lakes and >0.5 km for blue-water lakes). Lakes containing gray water also tended to be more elongated and often lay at the end of a glacier tongue (eg LCN161, 1040, 1056).

Water color variability was investigated on a finer scale for Lake Chola (LCN24), which has predominantly turquoise waters, captured by the GeoEye-1 acquisition concurrently with our in situ measurements. Figure 5A shows a map of the r_w values in the 545-nm band, and Figure 5B shows the correspondence between the r_w spectra measured in situ and derived from the satellite data. The r_w at 545 nm is lower near the inflow, higher along the southwestern shore, and intermediate along the northeastern shore—constituting 3 zones that can be roughly identified on the image. The average spectral signatures of these zones, measured in situ and derived from satellite data, are plotted in Figure 5B. The southwestern and northeastern parts of the lake have similar spectra, with a slight variability in magnitude (probably due to differences in their suspended sediment loads). The waters near the inflow show slightly lower r_w values for the blue-green wavelengths, suggesting the presence of light-absorbing substances entering the lake.

Discussion

The analysis of lake color in relation to size and shape showed differences that can be explained by the different origins of the lakes. Those with a more circular shape are usually cirque lakes, with a well-defined basin modeled by ancient glacier action and currently fed by river water or rain; lakes with an ellipsoid shape are more typically supraglacial and proglacial, formed directly by the melting of glacier tongues and adapting to their shape. Lakes with gray and turquoise water were found closer to glaciers than blue-water lakes, and their proximity to a glacier points to a possible link between lake water color and glacier melting. The elongated shape and increased surface area of a lake may be indicators of a glacial lake outburst flood risk. ICIMOD (2011) identified 10 lakes in Nepal with a high level of surveillance priority due to their physical parameters and socioeconomic factors. Our study found most (7 of 10) of these potentially dangerous lakes (LCN161, 1021, 1028, 1033, 1048, 1053, and 1059) to be gray in color and located 0 to 75 m from their respective glaciers, with a shape index higher than 0.4.

Some 116 lakes included in our study were also classified by water color in an earlier study (Giardino et al 2010); in general, these became more gray over the intervening 6 years. One possible reason for this trend is glacier shrinkage, which has been amply discussed as a

consequence of global climate change. Glacier surface area in the SNP shrank by 261 km^2 from 1980 to 2010 (ICIMOD 2014, 2015). The lowest elevation of glacier tongues has also shifted upward for 54% of the glaciers in the region, by an average of 40 m, and 97% of the glaciers have become thinner, on average by 7 m. All these data point to a retreating trend of the glaciers in the study area from 1980 to 2010 and support our hypothesis that glacier shrinkage influences water color in the region's glacial lakes.

With its high spatial resolution, the GeoEye-1 generated data capable of showing variations in water reflectance within a single lake (Figure 5). The mountain slopes on the southwestern and northeastern shores of this lake are quite different, the former mainly consisting of rocks and debris, the latter colonized by sparse vegetation (alpine pastures and shrubs). When the snow melts, the surface flow of water tends to carry some of the debris into the lake, and runoff erosion affects mainly less consolidated slopes, which are usually not covered by vegetation (Fattet et al 2011; Huang et al 2013), as in the case of the southwestern slope. This could explain why the reflectance values were higher on the southwestern side of the lake.

Conclusions

The present study combined in situ and satellite data to characterize the water color of Himalayan lakes in the SNP and surrounding area. In situ radiometric measures (WISP-3) and SD measurements enabled a distinction between 3 water color classes—blue, turquoise, and gray—coinciding with decreasing levels of water clarity and increasing levels of brightness. The comparison between the transparency measurements obtained with the SD and the iQwtr instrument seems promising (even though only 5 samples were available), and would support the future use of innovative app-based instrumentation in fieldwork.

The different spatial resolutions of satellite sensors proved adaptable to different aims, from more detailed analysis of the spatial distribution of the water characteristics in a given lake to mapping of the lakes on a regional scale. Most of the lakes in the study area were classified as having predominantly gray waters, and these lakes also seemed to have larger surface areas and elongated shapes, probably extending directly from the glacier tongue that feeds them—a combination that raises the risk of outburst flooding. When direct surface melting gives rise to small ponds on a glacier's surface that evolve into proglacial lakes, the water of the lake is dammed by the glacier's moraine, which cannot retain it securely in the event of an avalanche or damage to the moraine. Our comparison of data obtained in 2008 and 2014 showed a tendency for lake water to become less clear (more turquoise or gray than blue). The factors behind this change need to be investigated and discussed, but we already know that the past 40 years or so have seen the glaciers in the area (and specifically within the SNP) shrink in size and thickness, and the lowest edge of more than half of them has shifted to higher altitudes.

Satellite remote sensing is a good way to track glacier–lake interactions in scarcely accessible areas such as the Himalayas, but it has some limitations. One concerns the spatial resolution, which restricts the investigation of lakes smaller than the minimum mappable unit (image pixel). Another concerns the orography and adjacent bright lands, which hamper the extraction of pure signals reflected by water because of areas of shadow. With the Sentinel-2 now in orbit (capable of 10-m resolution and a 10-day revisiting time, which will drop to 5 days once the second Sentinel-2 is in orbit), better data are available for capturing the spatial and temporal variability of water color in the Himalayan region. Its 10- and 20-m spatial resolution bands are an important innovation, because spatial resolution remains one of the main factors limiting the application of satellite remote sensing to freshwater ecosystems (Ozesmi and Bauer 2002; Hestir et al 2015).

REFERENCES

Arendt A, Bliss A, Bolch T, Cogley JG, Gardner AS, Hagen O, Hock R, Huss M, Kaser G, Kienholz C, Pfeffer WT, Moholdt G, Paul F, Radić V, Andreassen L, et al. 2014. *Randolph Glacier Inventory – A Dataset of Global Glacier Outlines: Version 4.0.* Global Land Ice Measurements from Space. Boulder, CO: Digital Media.

Bajracharya B, Shrestha AB, Rajbhandari L. 2007. Glacial lake outburst floods in the Sagarmatha region – Hazard assessment using GIS and hydrodynamic modeling. *Mountain Research and Development* 27(4):336–344. http://dx.doi.org/10.1659/mrd.0783.

Bélanger S, Ehn JK, Babin M. 2007. Impact of sea ice on the retrieval of water-leaving reflectance, chlorophyll a concentration and inherent optical properties from satellite ocean color data. *Remote Sensing of Environment* 111:51–68. http://dx.doi.org/10.1016/j.rse.2007.03.013.

Bogaert J, Rousseau R, Van Hecke P, Impens I. 2000. Alternative area-perimeter ratios for measurement of 2D shape compactness of habitats.

Applied Mathematics and Computation 111(1):71–85. http://dx.doi.org/10.1016/S0096-3003(99)00075-2.

Bolch T, Buchroithner MF, Peters J, Baessler M, Bajracharya S. 2008. Identification of glacier motion and potentially dangerous glacial lakes in the Mt. Everest region/Nepal using spaceborne imagery. *Natural Hazards and Earth System Sciences* 8:1329–1340. http://dx.doi.org/10.5194/nhess-8-1329-2008.

Brando VE, Lovell JL, King EA, Boadle D, Scott R, Schroeder T. 2016. The potential of autonomous ship-borne hyperspectral radiometers for the validation of ocean color radiometry data. *Remote Sensing* 8(2):150. http://dx.doi.org/10.3390/rs8020150

Buchroithner MF, Jentsch G, Wanivenhaus B. 1982. Monitoring of recent geological events in the Khumbu area (Himalaya, Nepal) by digital processing of Landsat MSS data. *Rock Mechanics and Rock Engineering* 15(4):181–197. http://dx.doi.org/10.1007/BF01240589.

Bukata RP, Jerome JH, Kondrateyev KY, Pozdnyakov DV. 1995. *Optical Properties and Remote Sensing of Inland and Coastal Waters*. Boca Raton, FL: CRC Press.

Byers AC, McKinney DC, Somos-Valenzuela M, Watanabe T, Lamsal D. 2013. Glacial lakes of the Hinku and Hongu valleys, Makalu Barun National Park and Buffer Zone, Nepal. *Natural Hazards* 69(1):115–139. http://dx.doi.org/10.1007/s11069-013-0689-8.

Fattet M, Fu Y, Ghestem M, Ma W, Foulonneau M, Nespoulous J, Le Bissonnais Y, Stokes A. 2011. Effects of vegetation type on soil resistance to erosion: Relationship between aggregate stability and shear strength. *Catena* 87(1):60–69. http://dx.doi.org/10.1016/j.catena.2011.05.006.

Frohn RC. 2006. The use of landscape pattern metrics in remote sensing image classification. *International Journal of Remote Sensing* 27(9–10):2025–2032. http://dx.doi.org/10.1080/01431160500212229.

Ghezehegn SG, Steef P, Hommersom A, Nils D, Culcea O, Krommendijk B. 2014. Hyperspectral remote sensing for estimating coastal water quality: Case study on coast of Black Sea, Romania. *In:* Neale CMU, Maltese A, editors. *Remote Sensing for Agriculture, Ecosystems, and Hydrology XVI*. Proceedings of SPIE Vol 9239, Article No. 923913. http://dx.doi.org/10.1117/12.2067415.

Gholizadeh MH, Melesse AM, Reddi L. 2016. Spaceborne and airborne sensors in water quality assessment. *International Journal of Remote Sensing* 37(14):3143–3180. http://dx.doi.org/10.1080/01431161.2016.1190477.

Giardino C, Oggioni A, Bresciani M, Yan H. 2010. Remote sensing of suspended particulate matter in Himalayan lakes: A case study of alpine lakes in the Mount Everest region. *Mountain Research and Development* 30(2):157–168. http://dx.doi.org/10.1659/MRD-JOURNAL-D-09-00042.1.

Hestir EL, Brando VE, Bresciani M, Giardino C, Matta E, Villa P, Dekker AG. 2015. Measuring freshwater aquatic ecosystems: The need for a hyperspectral global mapping satellite mission. *Remote Sensing of Environment* 167:181–195. http://dx.doi.org/10.1016/j.rse.2015.05.023.

Hommersom A, Kratzer S, Laanen M, Ansko I, Ligi M, Bresciani M, Giardino C, Beltran J, Moore G, Wernand M, Peters S. 2012. An inter-comparison in the field between the new Wisp-3 and other radiometers (TriOS Ramses, ASD FieldSpec, and TACCS). *Journal of Applied Remote Sensing* 6(1):063615. http://dx.doi.org/10.1117/1.JRS.6.063615.

Hommersom A, Wernand MR, Peters S, Eleveld MA, van der Woerd HJ, Boer J. 2011. Spectra of a shallow sea-unmixing for class identification and monitoring of coastal waters. *Ocean Dynamics* 61(4):463–480. http://dx.doi.org/10.1007/s10236-010-0373-4.

Huang J, Zhao X, Wu P. 2013. Surface runoff volumes from vegetated slopes during simulated rainfall events. *Journal of Soil and Water Conservation* 68(4):283–295. http://dx.doi.org/10.2489/jswc.68.4.283.

ICIMOD [International Centre for Integrated Mountain Development]. 2011. *Glacial Lakes and Glacial Lake Outburst Floods in Nepal*. Kathmandu, Nepal: ICIMOD.

ICIMOD [International Centre for Integrated Mountain Development]. 2014. *Glaciers of Nepal 2010*. Kathmandu, Nepal: ICIMOD.

ICIMOD [International Centre for Integrated Mountain Development]. 2015. *Glaciers of Nepal 1980. Glaciers of Nepal 1990. Glaciers of Nepal 2000*. Kathmandu, Nepal: ICIMOD.

Irwin J. 1974. Water clarity records from twenty-two New Zealand lakes. *New Zealand Journal of Marine and Freshwater Research* 8(1):223–227. http://dx.doi.org/10.1080/00288330.1974.9515498.

Kargel JS, Abrams MJ, Bishop MP, Bush A, Hamilton G, Jiskoot H, Kääb A, Kieffer HH, Lee EM, Paul F, Rau F, Raup B, Shroder JF, Soltesz D, Stainforth D, et al. 2005. Multispectral imaging contributions to global land ice measurements from space. *Remote Sensing of Environment* 99(1):187–219. http://dx.doi.org/10.1016/j.rse.2005.07.004.

Kirk JTO. 2011. *Light and Photosynthesis in Aquatic Ecosystems*. 3rd edition. New York, NY: Cambridge University Press.

Koenings JP, Burkett RD, Edmundson JM. 1990. The exclusion of limnetic cladocera from turbid glacier-meltwater lakes. *Ecology* 71:57–67. http://dx.doi.org/10.2307/1940247.

Lami A, Marchetto A, Musazzi S, Salerno F, Tartari G, Guilizzoni P, Rogora M, Tartari GA. 2010. Chemical and biological response of two small lakes in the Khumbu Valley, Himalayas (Nepal) to short-term variability and climatic change as detected by long-term monitoring and paleolimnological methods. *Hydrobiologia* 648:189–205. http://dx.doi.org/10.1007/s10750-010-0262-3.

Mattson LE, Gardner JS, Young GJ. 1993. Ablation on debris covered glaciers: an example from the Rakhiot Glacier, Punjab, Himalaya. *In:* Young GJ, editor. *Snow and Glacier Hydrology*. IAHS Publication 218. Wallingford, United Kingdom: International Association of Hydrological Sciences, pp 289–296.

Odermatt D, Giardino C, Heege T. 2010. Chlorophyll retrieval with MERIS Case-2-Regional in perialpine lakes. *Remote Sensing of Environment* 114(3):607–617. http://dx.doi.org/10.1016/j.rse.2009.10.016.

Ozesmi SL, Bauer ME. 2002. Satellite remote sensing of wetlands. *Wetlands Ecology and Management* 10(5):381–402. http://dx.doi.org/10.1023/A:1020908432489.

Pahlevan N, Lee Z, Wei J, Schaaf CB, Schott JR, Berk A. 2014. On-orbit radiometric characterization of OLI (Landsat-8) for applications in aquatic remote sensing. *Remote Sensing of Environment* 154:272–284. http://dx.doi.org/10.1016/j.rse.2014.08.001.

Quincey DJ, Richardson SD, Luckman A, Lucas RM, Reynolds JM, Hambrey MJ, Glasser NF. 2007. Early recognition of glacial lake hazards in the Himalaya using remote sensing datasets. *Global and Planetary Change* 56(1):137–152. http://dx.doi.org/10.1016/j.gloplacha.2006.07.013.

Raj KBG, Kumar KV. 2016. Inventory of glacial lakes and its evolution in Uttarakhand Himalaya using time series satellite data. *Journal of the Indian Society of Remote Sensing* 44(6):959–976. http://dx.doi.org/10.1007/s12524-016-0560-y.

Raj KBG, Kumar VK, Remya SN. 2013. Remote sensing-based inventory of glacial lakes in Sikkim Himalaya: Semi-automated approach using satellite data. *Geomatics, Natural Hazards and Risk* 4(3):241–253. http://dx.doi.org/10.1080/19475705.2012.707153.

Robinson CT, Matthaei S. 2007. Hydrological heterogeneity of an alpine stream–lake network in Switzerland. *Hydrological Processes* 21(23):3146–3154. http://dx.doi.org/10.1002/hyp.6536.

Salerno F, Buraschi E, Bruccoleri G, Tartari G, Smiraglia C. 2008. Glacier surface-area changes in Sagarmatha National Park, Nepal, in the second half of the 20th century, by comparison of historical maps. *Journal of Glaciology* 54(187):738–752. http://dx.doi.org/10.3189/002214308786570926.

Tartari G, Salerno F, Buraschi E, Bruccoleri G, Smiraglia C. 2008. Lake surface area variations in the north-eastern sector of Sagarmatha National Park (Nepal) at the end of the 20th century by comparison of historical maps. *Journal of Limnology* 67(2):139–154. http://dx.doi.org/10.4081/jlimnol.2008.139.

Tartari G, Tartari GA, Valsecchi S, Camusso M. 1997. Cadastre and hydrochemistry of high altitude lakes in the Mount Everest region. *Verhandlungen - Internationale Vereinigung für theoretische und angewandte Limnologie* 26(2):397–402.

Thakuri S, Salerno F, Smiraglia C, Bolch T, D'Agata C, Viviano G, Tartari G. 2014. Tracing glacier changes since the 1960s on the south slope of Mt. Everest (central Southern Himalaya) using optical satellite imagery. *The Cryosphere* 8:1297–1315. http://dx.doi.org/10.5194/tc-8-1297-2014.

Thies H, Nickus U, Mair V, Tessadri R, Tait D, Thaler B, Psenner R. 2007. Unexpected response of high alpine lake waters to climate warming. *Environmental Science and Technology* 41:7424–7429. http://dx.doi.org/10.1021/es0708060.

Thompson SS, Benn DI, Dennis K, Luckman A. 2012. A rapidly growing moraine-dammed glacial lake on Ngozumpa Glacier, Nepal. *Geomorphology* 145–146:1–11. http://dx.doi.org/10.1016/j.geomorph.2011.08.015.

Ueno K, Fujii H, Yamada H, Liu L. 2001. Weak and frequent monsoon precipitation over the Tibetan Plateau. *Journal of the Meteorological Society of Japan* 79(1B):419–434. http://dx.doi.org/10.2151/jmsj.79.419.

Vermote E, Tanré D, Deuzé JL, Herman M, Morcrette JJ. 1997. Second Simulation of Satellite Signal in the Solar Spectrum, 6S: An overview. *IEEE Transactions on Geoscience and Remote Sensing* 35(3):675–686. http://dx.doi.org/10.1109/36.581987.

Vuichard D, Zimmermann M. 1987. The 1985 catastrophic drainage of a moraine-dammed lake, Khumbu Himal, Nepal: Cause and consequences. *Mountain Research and Development* 7(2):91–110. http://dx.doi.org/10.2307/3673305.

Wu SS, Yao ZJ, Huang HQ, Liu ZF, Liu GH. 2012. Responses of glaciers and glacial lakes to climate variation between 1975 and 2005 in the Rongxer basin of Tibet, China and Nepal. *Regional Environmental Change* 12:887–898. http://dx.doi.org/10.1007/s10113-012-0302-9.